2022

Modeling And Experiments On A Dedicated Outdoor Air System Using Liquid Desiccant Heat And Mass Exchangers

Jason Woods

Eric Kozubal

Peter Luttik

David Fox

Jason Warner

Modeling and experiments on a dedicated outdoor air system using liquid desiccant heat and mass exchangers

Jason WOODS[1]*, Eric KOZUBAL[1], Peter LUTTIK[2], David FOX[2], Jason WARNER[2]

[1] National Renewable Energy Laboratory, Golden, CO, USA
Contact information (Jason.woods@nrel.gov)

[2] Emerson Climate Technologies, Sidney, OH, USA
Contact information (Jason.warner@nrel.gov)

* Corresponding Author

ABSTRACT

Liquid desiccants can provide efficient dehumidification but have yet to see widespread adoption. Most systems studied previously use natural gas-combustion to heat and regenerate the desiccant, and a central chiller plant or cooling tower for removing the heat of absorption. Here we present modeling and experimental results on a novel packaged air conditioner integrating liquid-desiccant heat and mass exchangers with a vapor compression cycle. The packaged system does not need cold or hot water from a central plant or cooling tower and is suitable for rooftop unit air conditioners. The system uses the evaporator to cool the liquid desiccant that is absorbing moisture from the air, and the condenser to heat the liquid desiccant to regenerate it. Efficiency is improved by reducing the load on the evaporator for a given supply-air dewpoint. This paper presents the measured dehumidification efficiency for a 10-ton packaged air conditioner, focusing on dehumidifying ventilation air. The paper also presents a numerical model to predict the outlet conditions and dehumidification efficiency, which we compare with the measured data.

1. INTRODUCTION

Ensuring the health and comfort of building occupants requires ventilation. This is typically provided by mixing outdoor air into the return air for each air conditioner of a building. An alternative is to use a dedicated outdoor air system (DOAS), which conditions all outdoor ventilation air for a building, leaving the non-ventilation load for the primary air conditioners. This approach ensures indoor air quality by providing adequate ventilation, and it can simplify the primary air conditioning system by limiting the psychrometric conditions that it sees (Larranaga *et al.*, 2008). In humid climates, this reduces the latent (i.e., humidity) load on the primary air conditioners, enabling sensible-only cooling options like efficient high-airflow systems or radiant-based cooling (Coad, 1999).

A DOAS must efficiently handle all inlet ambient conditions. This is becoming challenging as building efficiency improves, which lowers the sensible loads but does not impact the latent load. Better insulation reduces sensible heat gains from ambient and more efficient lighting reduces internal sensible heat gains. But the internal gains from people and their activities, and the ventilation humidity load have not changed. This new balance between sensible and latent loads means a DOAS in a humid climate must provide efficient humidity control without overcooling the building.

Different options exist for this high-latent cooling DOAS, including over-cool reheat (Ling *et al.*, 2008), desiccant wheels (Hwang *et al.*, 2010), vacuum-driven membrane dehumidification (Woods, 2014), and liquid desiccant systems (Lowenstein, 2008). Here we focus on the use of liquid desiccant heat and mass exchangers (HMXs), which use aqueous salt solutions with low equivalent water-vapor pressures. This low vapor pressure is used to dehumidify air without the need for cooling to the dewpoint. The analyzed system couples liquid desiccant HMXs with a vapor compression system. It is a 'packaged' system, meaning it is a like-for-like replacement of existing vapor-compression DOAS. It uses two 3-fluid HMXs: one to dehumidify ventilation air (cooled by the evaporator), and one to regenerate the desiccant (heated by the condenser). The 3-fluid HMXs have a parallel-plate geometry with air and liquid desiccant separated by a porous membrane, and the liquid desiccant and cooling or heating water separated by a plastic plate.

The proposed addition of liquid desiccant HMXs to a vapor-compression cycle reduces energy use compared to the typical overcool-reheat approach. The heat load passing through the compressor is lower because the liquid desiccant provides the same level of dehumidification without requiring the air to be cooled to the dewpoint.

Several researchers have explored using liquid desiccants for dehumidification. Many of these use liquid desiccants with heated or cooled from a central heating or cooling plant (Xiao *et al.*, 2011, Ou *et al.*, 2018) or from natural-gas combustion and a cooling tower (Woods and Kozubal, 2013). These approaches require additional connections (e.g., chilled-water or natural gas line) that do not allow for a like-for-like replacement of existing rooftop air conditioners. Others have investigated 2-fluid HMXs (no coolant flow) coupled with a vapor compression cycle. These include ones with a packed tower (Niu *et al.*, 2012, Zhang *et al.*, 2012) or a membrane exchanger (Zhang *et al.*, 2016, Abdel-Salam and Simonson, 2020). Because the HMXs have only two fluids (liquid desiccant and air), the liquid desiccant is cooled or heated external from the HMX. Using internally-cooled HMXs instead lowers the liquid desiccant flow rates and pumping power can improve efficiency by minimizing heat-pump temperature lift. Previous studies reported on a vapor-compression cycle with 3-fluid HMXs: two with refrigerant tubes cooling a packed tower of liquid desiccant (Yamaguchi *et al.*, 2011, Liu *et al.*, 2020), and one where a refrigerant cools a desiccant channel with embedded hollow-fiber membranes for airflow (Isetti *et al.*, 2013). These systems, and the systems with 2-fluid HMXs that use a refrigerant-to-desiccant heat exchanger, require expensive metals to avoid corrosion but still reach the pressures required by the refrigerant. The system investigated here uses water-to-refrigerant heat exchangers with the water stream within the 3-fluid HMX, which allows for the use of low-pressure polymer HMXs and standard

Here we present the performance of this packaged liquid desiccant system for conditioning ventilation air. We present a numerical model that was used to design the system and the experimental results on a 10-ton prototype for a range of ambient conditions. We also present the measured and modeled dehumidification efficiency of the system for different inlet and outlet conditions.

2. METHODS

2.1 System description

The packaged, liquid desiccant HMX system (Figure 1) includes:

- A refrigeration sub-system: compressor, condenser, evaporator, and expansion valve
- A desiccant sub-system: conditioner and regenerator HMXs, desiccant-to-desiccant heat exchanger
- Fans and pumps for moving air, water, or liquid desiccant

The refrigeration system provides chilled water to the conditioner HMX. The conditioner dehumidifies and cools the incoming ventilation air using this chilled water and the concentrated liquid desiccant. The heat absorbed into the chilled water is ultimately rejected through the condenser of the refrigeration system. This heat is used to re-concentrate the liquid desiccant in the regenerator by evaporating water from the desiccant.

Using the liquid desiccant HMXs, instead of direct-expansion or water-cooled heat exchange coils, reduces the system's sensible heat ratio (SHR). Additional components can be added to the system in Figure 1 to enable better control over temperature or humidity. Future publications will expand upon these alternative configurations and their control strategies, but are outside of the scope of this paper.

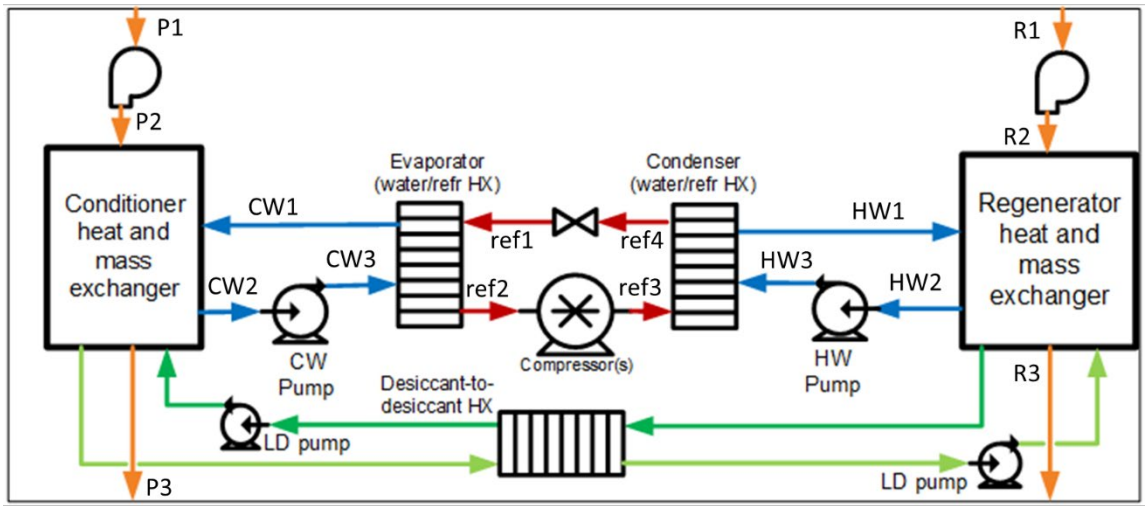

Figure 1: System schematic. HW=hot water, CW=chilled water, ref=refrigerant, P=process air, R=regeneration air.

2.2 10-ton prototype and experiments

A 10-ton prototype system (Figure 2) was built per the design shown in Figure 1. The components include:

- An Emerson variable-speed scroll compressor
- SWEP brazed-plate condenser and evaporator heat exchangers, sized for ~1.5-2 °C approach temperature
- A counterflow, parallel-plate desiccant-to-desiccant heat exchanger
- Variable-speed pumps for the hot and cold water and liquid desiccant
- The conditioner and regenerator, which each have 145 air channels and a nominal face velocity of 1.9 m/s (374 ft/min). This 3-fluid design is described in Woods and Kozubal (2018).
- Variable speed plenum fans for the conditioner and regenerator airflow.

We characterized the prototype system in a psychrometric room that simulated outdoor conditions by controlling dry bulb temperature with heating and cooling coils, and humidity with spray nozzles. The outlet of both the regenerator and conditioner returned to the room. High velocity fans along the ceiling and floor ensured adequate mixing of inlet air, which we verified by measuring temperature and humidity at both the conditioner and regenerator HMX inlets. The system delivered air at 1500 ft^3/min (2548 m^3/hr). An additional 1 inH_2O (249 Pa) pressure drop was added to the conditioner-side airflow to simulate the static pressure drop of ductwork in an actual installation.

Temperature sensors (4-wire PT100 RTD's) were located on all fluid streams (refrigerant, water, desiccant, air) before and after each component: liquid desiccant HMXs, water-refrigerant heat exchangers, desiccant-to-desiccant heat exchanger, and compressor. We calibrated these in-situ using a dry-block calibrator. Dry bulb and wet bulb measurements were recorded using aspirated psychrometers, which pulled air out of the PVC sampling trees at the inlet and outlet of the conditioner and regenerator (Figure 2). Air flow was measured within the outlet duct of the conditioner and regenerator using an array of anemometers, with NIST-traceable calibrations. Ohio Semitronics power meters measured total electric power and individual power for the compressor, water pumps, and two fans. The liquid desiccant pumps were included in the total electric power, but not separately metered.

We calculated two energy balances to ensure data quality. The first is an energy balance on the conditioner, comparing the total cooling of the air with the energy change of the water and desiccant flows. This also considers the exothermic heat generated from the enthalpy of dilution as the desiccant concentration changes. The second uses a control volume around the entire system, and compares the total cooling of the conditioner air with the heat rejected by the regenerator and the electric power input into the unit. These differences were within 5% and 10%, respectively, for each experiment. A moisture balance was also calculated comparing the water vapor absorbed out of the conditioner air to the water vapor released into the regenerator air. The moisture balance was within 15%. This means that, in some cases, the desiccant concentration was still changing slowly during the experiment, but this difference is low enough to still be representative of the system performance at the measured conditions.

Nominal flow rates for this system are, air: 2550 m^3/h, water: 70 L/min, and liquid desiccant: 5 L/min.

Figure 2: DOAS unit in psychrometric room. Psychrometers shown on regenerator (left) and conditioner (right) inlets.

2.3 Modeling

2.3.1 Refrigeration components

The refrigeration system includes the compressor, evaporator, condenser, and expansion valve. Properties for the refrigerant (R410a) are from Lemmon (2003). We assume the following for modeling the refrigeration system:

- The refrigerant is isenthalpic (constant enthalpy) through the expansion valve.
- The superheated refrigerant exiting the evaporator ($T_{ref,2}$) is controlled by the expansion valve to 5 °C above the saturated evaporator temperature ($T_{ref,sat,evap}$): $T_{ref,2} = T_{ref,sat,evap} + 5\ ℃$
- The subcooled refrigerant exiting the condenser ($T_{ref,4}$) exits 75% of the way from the saturated condensing temperature ($T_{ref,sat,cond}$) to the entering water temperature ($T_{HW,1}$): $T_{ref,4} = T_{ref,sat,cond} - 0.75\left(T_{ref,sat,cond} - T_{HW,1}\right)$
- There is negligible pressure-loss for the refrigerant in heat exchangers and piping

Compressor: The variable-speed compressor is modeled using a 20-coefficient regression model from Emerson Climate Technologies (Emerson, 2020), which outputs refrigerant mass flow rate and input electric power, including losses from the variable-frequency drive. The regression equations are of the form:

$$\dot{m}_{ref} = f\left(T_{ref,evap,sat}, T_{ref,cond,sat}, RPM_{compr}\right) \quad (1)$$

$$W_{elec,compr} = f\left(T_{ref,evap,sat}, T_{ref,cond,sat}, RPM_{compr}\right) \quad (2)$$

where RPM_{compr} is the compressor speed in revolutions per minute. The mass flow rate and compressor power from these regressions are adjusted by the superheat ($\Delta T_{ref,evap,SH}$), which impacts the refrigerant density entering the compressor, compared to the assumed $\Delta T_{ref,evap,SH}$ used to create the regression.

Evaporator and condenser heat exchangers: The refrigerant-to-water heat exchangers are modeled with a number-of-transfer-units (NTU)-effectiveness relation for counterflow heat exchangers. The NTU is:

$$NTU = \frac{UA}{(\dot{m}c_p)_{min}} \quad (3)$$

where U is the overall heat transfer coefficient, A the heat exchange surface area, and $\dot{m}$ and c_p the mass flow rate and specific heat of the minimum heat-capacity fluid. The effectiveness for the single- and two-phase flows are:

Single-phase refrigerant or water: $$\varepsilon = \frac{1-exp[-NTU(1-C_r]}{1-C_r exp[-NTU(1-C_r]} \quad (4)$$

Two-phase refrigerant: $$\varepsilon = 1 - \exp\left(-NTU\right) \quad (5)$$

where C_r is the heat capacity ratio:

$$C_r = \frac{(\dot{m}c_p)_{min}}{(\dot{m}c_p)_{max}} \quad (6)$$

The subscript *min* indicates the lower heat capacity (either water or refrigerant) and the subscript *max* indicates the other heat capacity. In the model, the overall heat transfer coefficient, U, is calculated with a resistance network:

$$U = \left[\frac{1}{h_{w,conv}} + \left(\frac{\delta_{plate}}{k_{plate}}\right) + \frac{1}{h_{ref,conv}}\right]^{-1} \quad (7)$$

where the three terms are the water-side convective heat transfer resistance, the plate conductive resistance (thickness divided by conductivity), and the refrigerant-side convective resistance. The model calculates U for each region in these heat exchangers (Figure 3(a)), including single-phase superheated or subcooled refrigerant and two-phase boiling or condensing refrigerant. The heat transfer coefficients are calculated with correlations for single-phase, two-phase boiling, or two-phase condensing using correlations for chevron-plate channels from Muley and Manglik (1999), Donowski and Kandliker (2000), and Yan *et al.* (1999). The surface area for each region sums to the total heat exchanger surface area. These areas change depending on the refrigerant densities at the operating conditions.

After calculating the effectiveness for each region (Eqs. (3-7)), we calculate outlet temperatures with the equations below. In these equations, $Q_{evap,SH}$, $Q_{cond,SH}$, and $Q_{cond,SC}$ are the heat transfer rates in the evaporator superheated region, condenser superheated region, and condenser subcooled region, respectively. The subscripts used in the chilled and hot water temperatures depict the locations as shown in Figure 3.

Evaporator 2-phase refrigerant: $$T_{CW,1} = T_{CW,3a} + \varepsilon_{evap,sat}\left(T_{CW,3a} - T_{ref,evap,sat}\right) \quad (8)$$

Evaporator superheated vapor: $$T_{CW,3a} = T_{CW,3} + Q_{evap,SH}/\dot{m}_{CW}c_{p,CW} \quad (9)$$

$$Q_{evap,SH} = \varepsilon_{evap,SH}\left(\dot{m}c_p\right)_{min,evap}\left(T_{CW,3} - T_{ref,evap,sat}\right) \quad (10)$$

Condenser superheated vapor: $$T_{HW,1} = T_{HW,3b} + Q_{cond,SH}/\dot{m}_{HW}c_{p,HW} \quad (11)$$

$$Q_{cond,SH} = \varepsilon_{cond,SH}\left(\dot{m}c_p\right)_{min,cond,SH}\left(T_{HW,3b} - T_{ref,3}\right) \quad (12)$$

Condenser 2-phase refrigerant: $$T_{HW,3b} = T_{HW,3a} + \varepsilon_{cond,sat}\left(T_{HW,3a} - T_{ref,cond,sat}\right) \quad (13)$$

Condenser subcooled liquid: $$T_{HW,3a} = T_{HW,3} + Q_{cond,SC}/\dot{m}_{HW}c_{p,HW} \quad (14)$$

$$Q_{cond,SC} = \varepsilon_{cond,SH}\left(\dot{m}c_p\right)_{min,cond,SC}\left(T_{HW,3} - T_{ref,cond,sat}\right) \quad (15)$$

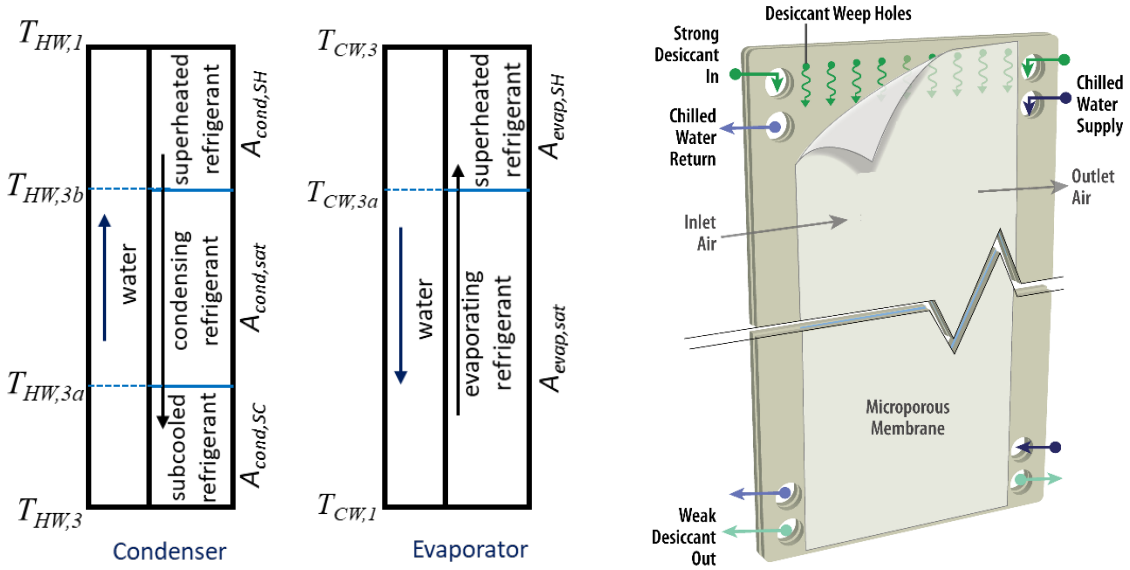

Figure 3*:* Schematics of (a) condenser and evaporator heat exchangers, (b) 3-fluid liquid desiccant HMX.

2.3.2 Liquid desiccant components

Liquid desiccant HMXs: The system uses internally cooled HMXs (Figure 3(b)) consisting of repeating sets of parallel channels. The water provides either heating for regeneration or cooling for dehumidification. The models for the conditioner and regenerator are the same, but the directions of heat and mass transfer differ due to the directions of the driving forces. In the conditioner, the desiccant is cooled, lowering its equivalent vapor pressure, setting up a mass-transfer driving force from the air to the desiccant. In the regenerator, the desiccant is heated, raising its equivalent vapor pressure, setting up a mass-transfer driving force from the desiccant to the air. Properties for the desiccant (LiCl) are from Conde (2004). The HMX finite-difference model for this HMX were previously described in Woods and Kozubal (2018). It takes as inputs the flows and temperatures for air, desiccant, and water, as well as the desiccant concentration and air humidity. It returns these same properties at the HMX outlet back to the system model.

Desiccant-to-desiccant heat exchanger: The heat exchanger between the regenerator inlet and outlet desiccant streams recovers the heat added to the desiccant in the regenerator. This is modeled as a counter-flow heat exchanger with the same NTU-effectiveness equations as shown in Eqs. (3-5). The heat exchanger is sized to give an effectiveness of 0.85 at the design desiccant flow rate of 5 L/min.

2.3.3 Fans and pumps

The power draw of the fans and pumps depends on the pressure drop of each component. The electric power is this pressure drop times the flow rate, divided by the efficiency. Empirical correlations for pressure drop versus flow were developed for water flow through the condenser and evaporator heat exchangers, while pressure drop for air and water through the conditioner and regenerator are estimated based on the friction factor correlation for laminar flow in parallel-plate channels (f = 96/Re). The airside pressure drop also includes entrance and exit pressure effects, as described in Rohsenow *et al.* (1985):

$$\Delta P_{air,HMX} = \frac{f}{2}\rho V^2 + \frac{1}{2}\rho V^2(1-\sigma^2+K_{contr})\frac{1}{2}\rho V^2\left(1-\sigma^2+K_{exp}\right) \quad (16)$$

where V is the air channel velocity, σ is the ratio of the air channel open area to the total face area of the HMX, and K_{contr} and K_{exp} are the contraction and expansion pressure coefficients for flow into and out of an abrupt channel (K_{contr} = 0.75 and K_{exp} = 0.23, from Rohsenow *et al.* (1985)). For fans, we used a correlation derived from measured data, which predicts electric power as a function of flow rate, pressure drop, and air density. We assume 100% of the electric energy from the motor and fan heat the airstream. For pumps, we used a correlation derived from measured data, which predicts electric power as a function of flow rate and pressure drop. We assume 50% of the electrical energy from the pump enters the liquid stream (50% is lost to ambient).

2.3.4 Model implementation

Fluid properties for air and water are based on built-in functions within the Engineering Equation Solver (EES) platform (Klein, 2019). The above equations, including the finite-difference equations for the HMXs from Woods and Kozubal (2018), were written into the EES program and solved simultaneously through the Newton-Raphson method, using a set of guess values for each variable, and then iterating until the relative residuals are less than $1x10^{-6}$.

2.4 Performance assessment

The performance of a DOAS is measured by the dehumidification efficiency, which is the mass of water vapor removed from the air divided by the energy input. We calculate this based on both the system total electric power (W_{total}), and the compressor electric power ($W_{compressor}$):

$$\text{Dehumidification efficiency} = \frac{\dot{m}_{dryair,P}(\omega_{P,1}-\omega_{P,3})}{W_{total}} \quad (17)$$

$$\text{Compressor dehumidification efficiency} = \frac{\dot{m}_{dryair,P}(\omega_{P,1}-\omega_{P,3})}{W_{compressor}} \quad (18)$$

where $\dot{m}_{dryair,P}$ is the process-air flow rate on a dry-air basis, and $\omega_{P,1}$ and $\omega_{P,3}$ are the inlet and outlet humidity ratio of the process air. The system electric power includes the compressor, conditioner and regenerator fans, chilled-water and hot-water pumps, and the two desiccant pumps. Two other important metrics are the supply temperature and humidity. Some applications require lower humidity than others, and the supply temperature should not be too low to avoid over-cooling the space. In this paper, we investigate the performance for four inlet conditions:

Case 1. Hot/humid: 35 °C dry-bulb temperature, 22 °C dew point
Case 2. Warm/humid: 27 °C dry-bulb temperature, 21 °C dew point
Case 3. Mild/humid: 21 °C dry-bulb temperature, 18 °C dew point
Case 4. Cool/humid: 17 °C dry-bulb temperature, 14 °C dew point

Experiments were performed at these conditions to deliver air at 12 °C dewpoint (except for case 4, where the supply dewpoint is lower due to the relatively dry inlet conditions). We compare the modeling results to these four cases and use the model to explore the performance at drier outlet conditions.

3. RESULTS AND DISCUSSION

3.1 Cooling and dehumidification performance

The performance for the four cases is shown on a psychrometric chart in Figure 4. The solid lines are the model output and the dashed line are the prototype experimental data. Case 1 (top-left) includes labels for the different state points and airflows. For that case, the outdoor air (35 °C dry-bulb, 22 °C dew point) enters both the conditioner and regenerator. In the conditioner, the air is driving towards the equilibrium condition of the liquid desiccant, labeled as the *conditioner potential*. This potential is the humidity ratio of air in equilibrium with the liquid desiccant at the inlet liquid desiccant concentration and the temperature of the inlet chilled water. Because the liquid desiccant flow is 5-10% of the water flow, the inlet desiccant temperature is much less important than the water inlet temperature. The proposed system provides more latent cooling than a conventional system (SHR = 0.29 vs. SHR ~ 0.5 for a conventional system at Case 1 conditions). The regenerator air similarly approaches the *regenerator potential*, which is the humidity ratio of air in equilibrium with the liquid desiccant at the inlet hot-water temperature and the inlet desiccant concentration. The curved green lines, where the regenerator and conditioner potential points reside, are the equilibrium humidity for the liquid desiccant at the concentration entering the conditioner or regenerator. For simplicity, only one line is shown, but the inlet regenerator concentration is typically 1-2% concentration points, by weight, lower than the conditioner concentration.

Referring to Figure 4, the experiments reach 93-99% of the total cooling estimated by the model for each case, and 95-97% of the latent cooling for cases 1 to 3. For case 4, the prototype provided 10% more latent cooling than predicted by the model. This is partially explained by the higher concentration (and therefore lower equilibrium humidity) for the experiment in Case 4 since a higher concentration will provide more latent cooling. The conditioner potentials predicted by the model also align with the experiment, but the regenerator potential does not—the entering hot-water temperature for the experiments was consistently higher than the model predicted. This is indicative of a regenerator that is not performing as well as the model predicted; it requires higher temperatures to reach the same desiccant concentration as the model. This impacts the overall efficiency, as discussed below.

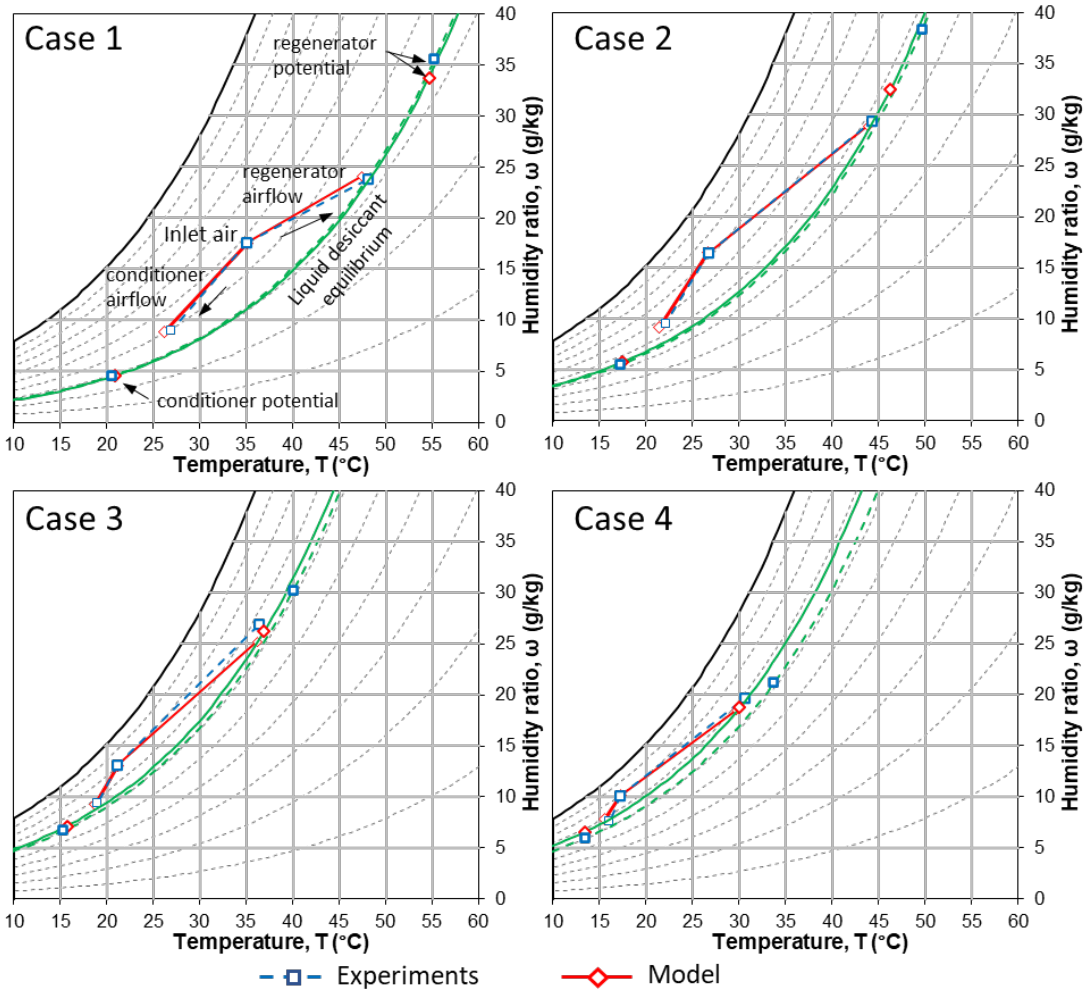

Figure 4: Psychrometric inlet and outlet conditions for the four cases. Labels are included in Case 1 (top left), but not in other cases for readability. Both modeled (solid line) and experiments (dashed line) are included.

Figure 5 shows an example T-s diagram for the refrigeration system (Case 2). The evaporator temperature (~14 °C) is higher than a standard vapor-compression system, helping to minimize temperature lift. The supply air temperature (~21 °C) is also higher than a standard system. This is beneficial for this case, where the ambient temperature is only slightly above room temperature and thus there is little need for sensible cooling. The experiments show higher saturated condenser and evaporator temperatures than the model prediction. For the condenser, this is consistent with the higher hot-water temperature in the regenerator. For the evaporator, the chilled-water temperature is slightly less than the model, but most of the difference between modeled and measured evaporator refrigerant temperatures is from the higher measured approach temperature (3.8 °C) for the evaporator compared to that predicted by the model (1.5 °C). After the experiments, we determined that the inlet tubing diameter selected for the evaporator was too large, causing poor refrigerant distribution. This was confirmed with later experiments on a new evaporator with a smaller diameter inlet header, where performance more closely matched the model. Unfortunately, this was not addressed until after the completion of the experiments on this 10-ton prototype system.

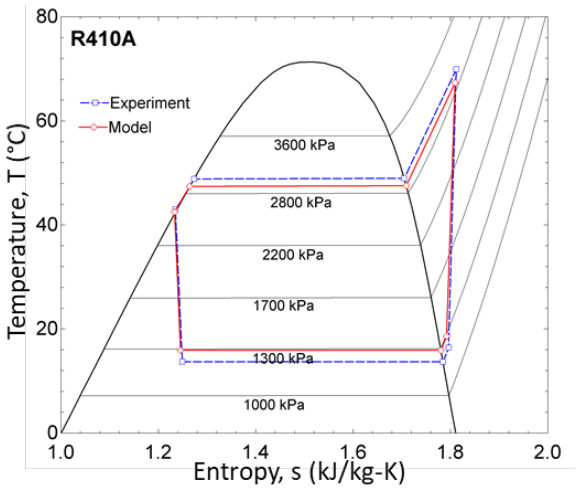

Figure 5: T-s diagram for Case 2, showing experiment (dashed line) and modeling (solid) state points.

3.2 Dehumidification efficiency – model measured comparison

The dehumidification efficiency is the moisture removal from the conditioner airstream (kg/hr) divided by the electric energy input (kW). Based on the total dehumidification provided (Figure 4) and the corresponding electric power, we calculated the dehumidification efficiency for each case. Figure 8a shows this efficiency based on the total electric power and the compressor electric power. The compressor-only efficiency is lower than the model prediction by an average of 9.5%, and a maximum of 15%. This is due to the larger temperature lift in the experiments compared to the model. The total system efficiency is based on the total input electric power, including fans and pumps. This dilutes the importance of the compressor, making the difference between model and experiments on average 4%, with the efficiency 6-9% lower for cases 1 to 3, and 9% higher for case 4. The case 4 discrepancy is due both to a higher compressor dehumidification efficiency, and because the fan and pump powers are more important for this low-load case. The compressor dehumidification efficiency is higher for case 4 because the latent cooling provided is higher than the model prediction (Figure 4).

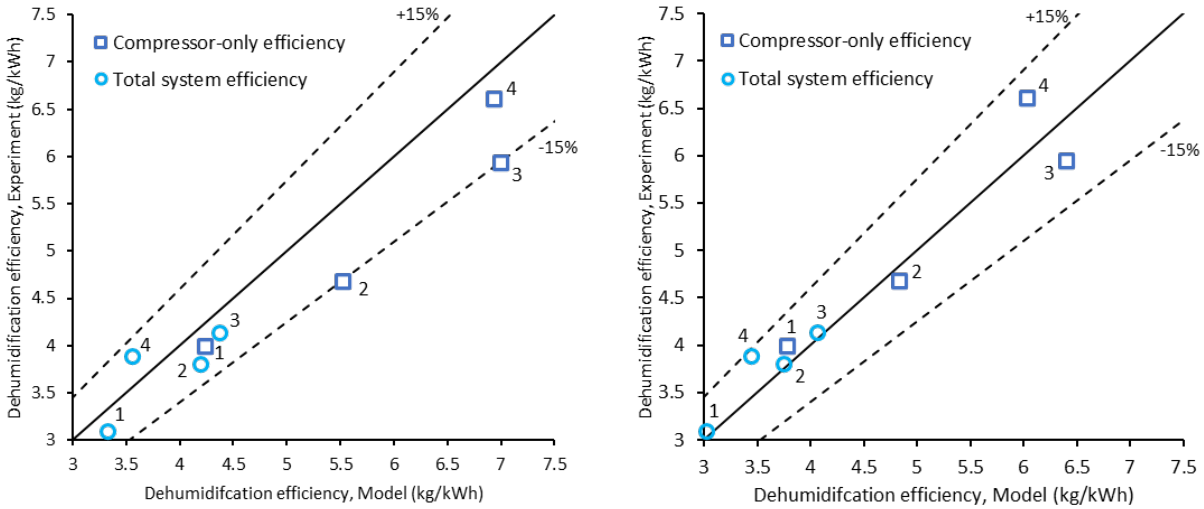

Figure 6: Dehumidification efficiency (model prediction compared to experiments) for the packaged DOAS system with liquid desiccant HMXs. (a) baseline model and (b) calibrated model.

The key drivers reducing the dehumidification efficiency below the model prediction is the high approach temperature of the evaporator, and the lower performance of the regenerator. Based on component-level performance, we can calibrate these two aspects of the model to better match the experiments. This calibration included lowering the latent effectiveness of the regenerator by 15% and reducing the evaporator heat exchanger *UA* by 40%. This calibrated model is compared to the data in Figure 8b, which reduces the average discrepancy for the compressor-only efficiency to 1%, and the total efficiency is then 4% over-predicted on average (primarily due to Case 4).

4. CONCLUSIONS

The packaged 10-ton prototype described in this paper has three key features: (1) it improves dehumidification efficiency of a vapor-compression cycle by reducing the load on the evaporator, (2) it improves humidity control by lowering the system's SHR, and (3) it accomplishes this without the need for a connection to a cooling tower, a natural gas line, or a central chilled or hot water loop.

The experimental results demonstrated the above three features and showed the potential of this system as a high-latent DOAS rooftop unit. The experiments matched the model well (efficiency predicted within 10%), with the largest discrepancies from an underperforming refrigerant-to-water evaporator, and a lower-than-predicted latent effectiveness for the regenerator. These raise the temperature lift, and therefore pressure ratio across the compressor, increasing power required. The gap between the model and the experiments was improved by calibrating the evaporator and regenerator performance. These results show sufficient accuracy to empower the model as an exploratory and design tool for predicting the performance of this desiccant technology.

Future research will explore the independent control of temperature and humidity with the proposed. There is also a need to quantify the performance of the system over a wider range of inlet conditions.

NOMENCLATURE

c_p	specific heat capacity	(J kg^{-1} K^{-1})
C_r	ratio of heat capacities	(W K^{-1})
δ	thickness	(m)
ε	heat exchanger effectiveness	(-)
k	thermal conductivity	(W m^{-1} K^{-1})
h	heat transfer coefficient	(W m^{-2} K^{-1})
$\dot{m}$	mass flow rate	(kg s^{-1})
N_{ch}	number of channels	(-)
NTU	number of transfer units	(-)
s	entropy	(J kg^{-1} K^{-1})
T	temperature	(°C)
U	overall heat transfer coefficient	(W K^{-1})
W	electric work	(kW)

Subscripts

cond	condenser of refrigeration system
conv	convection
CW	chilled water
evap	evaporator of refrigeration system
HW	hot water
ref	refrigerant
sat	saturated liquid/vapor mixture

REFERENCES

Abdel-Salam, A. H. and C. J. Simonson (2020). "Optimal design, sizing and operation of heat-pump liquid desiccant air conditioning systems." Science and Technology for the Built Environment **26**(2): 161-176.

Coad, W. (1999). "Conditioning Ventilation Air for Improved Performance and Air Quality." Heating, Piping and Air Conditioning(September 1999).

Conde, M. R. (2004). "Properties of aqueous solutions of lithium and calcium chlorides: formulations for use in air conditioning equipment design." International Journal of Thermal Sciences **43**(4): 367-382.

Donowski, V. and S. Kandliker (2000). Correlating evaporation heat transfer coefficient of refrigerant R-134a in a plate heat exchanger. Engineering Foundation Conference on Pool and Flow Boiling. Alaska.

Emerson. (2020). "Copeland Online Product Information." from https://climate.emerson.com/online-product-information/opiinterfaceservlet.

Hwang, Y., O. Kuwabara, J. Ling and R. Radermacher (2010). Enhancement of the separate sensible and latent cooling air-conditioning systems. International Refrigeration and Air Conditioning Conference West Lafayette, IN, Purdue University.
Isetti, C., E. Nannei and B. Orlandini (2013). "Three-fluid membrane contactors for improving the energy efficiency of refrigeration and air-handling systems." International Journal of Ambient Energy **34**(4): 181-194.
Klein, S. A. (2019). Engineering Equation Solver (EES). Madison, WI, F-Chart Software.
Larranaga, M., M. Beruvidas, H. W. Holder, E. Karunasena and D. Straus (2008). "DOAS & Humidity Control." ASHRAE Journal **May 2008**.
Lemmon, E. W. (2003). "Pseudo-Pure Fluid Equations of State for the Refrigerant Blends R-410A, R-404A,R-507A, and R-407C." International Journal of Thermophysics **24**(4): 991-1006.
Ling, J., Y. Hwang and R. Radermacher (2008). Theoretical study on separate sensible and latent cooling air-conditioning system. International Refrigeration and Air Conditioning Conference. West Lafayette, IN, Purdue University.
Liu, J., X. Liu and T. Zhang (2020). "Performance of heat pump driven internally cooled liquid desiccant dehumidification system." Energy Conversion and Management **205**: 112447.
Lowenstein, A. (2008). "Review of Liquid Desiccant Technology for HVAC Applications." HVAC&R Research **14**(6): 819-839.
Muley, A. and R. M. Manglik (1999). "Experimental Study of Turbulent Flow Heat Transfer and Pressure Drop in a Plate Heat Exchanger With Chevron Plates." Journal of Heat Transfer **121**(1): 110-117.
Niu, X., F. Xiao and Z. Ma (2012). "Investigation on capacity matching in liquid desiccant and heat pump hybrid air-conditioning systems." International Journal of Refrigeration **35**(1): 160-170.
Ou, X., W. Cai, X. He and D. Zhai (2018). "Experimental investigations on heat and mass transfer performances of a liquid desiccant cooling and dehumidification system." Applied Energy **220**: 164-175.
Rohsenow, W. M., J. P. Hartnett and E. N. Ganic (1985). Handbook of heat transfer fundamentals. New York, McGraw-Hill.
Woods, J. (2014). "Membrane processes for heating, ventilation, and air conditioning." Renewable and Sustainable Energy Reviews **33**(0): 290-304.
Woods, J. and E. Kozubal (2013). "A desiccant-enhanced evaporative air conditioner: Numerical model and experiments." Energy Conversion and Management **65**: 208-220.
Woods, J. and E. Kozubal (2018). "On the importance of the heat and mass transfer resistances in internally-cooled liquid desiccant dehumidifiers and regenerators." International Journal of Heat and Mass Transfer **122**: 324-340.
Xiao, F., G. Ge and X. Niu (2011). "Control performance of a dedicated outdoor air system adopting liquid desiccant dehumidification." Applied Energy **88**(1): 143-149.
Yamaguchi, S., J. Jeong, K. Saito, H. Miyauchi and M. Harada (2011). "Hybrid liquid desiccant air-conditioning system: Experiments and simulations." Applied Thermal Engineering **31**(17): 3741-3747.
Yan, Y.-Y., H.-C. Lio and T.-F. Lin (1999). "Condensation heat transfer and pressure drop of refrigerant R-134a in a plate heat exchanger." International Journal of Heat and Mass Transfer **42**(6): 993-1006.
Zhang, L., E. Hihara and M. Saikawa (2012). "Combination of air-source heat pumps with liquid desiccant dehumidification of air." Energy Conversion and Management **57**: 107-116.
Zhang, N., S.-Y. Yin and L.-Z. Zhang (2016). "Performance study of a heat pump driven and hollow fiber membrane-based two-stage liquid desiccant air dehumidification system." Applied Energy **179**: 727-737.

ACKNOWLEDGEMENT

This work was authored by the National Renewable Energy Laboratory, operated by Alliance for Sustainable Energy, LLC, for the U.S. Department of Energy (DOE) under Contract No. DE-AC36-08GO28308. Funding provided through a Cooperative Research and Development Agreement (CRADA) with 7AC Technologies (CRD-13-512). The views expressed in the article do not necessarily represent the views of the DOE or the U.S. Government. The U.S. Government retains and the publisher, by accepting the article for publication, acknowledges that the U.S. Government retains a nonexclusive, paid-up, irrevocable, worldwide license to publish or reproduce the published form of this work, or allow others to do so, for U.S. Government purposes.